

Article

Racemization of Serine Residues Catalyzed by Dihydrogen Phosphate Ion: A Computational Study

Ohgi Takahashi *, Ryota Kirikoshi and Noriyoshi Manabe

Faculty of Pharmaceutical Sciences, Tohoku Medical and Pharmaceutical University, 4-4-1 Komatsushima, Aoba-ku, Sendai 981-8558, Japan; kirikoshi@tohoku-mpu.ac.jp (R.K.); manabe@tohoku-mpu.ac.jp (N.M.)

* Correspondence: ohgi@tohoku-mpu.ac.jp; Tel.: +81-22-727-0208

Received: 26 October 2017; Accepted: 22 November 2017; Published: 27 November 2017

Abstract: Spontaneous, nonenzymatic reactions in proteins are known to have relevance to aging and age-related diseases, such as cataract and Alzheimer's disease. Among such reactions is the racemization of Ser residues, but its mechanism *in vivo* remains to be clarified. The most likely intermediate is an enol. Although being nonenzymatic, the enolization would need to be catalyzed to occur at a biologically relevant rate. In the present study, we computationally found plausible reaction pathways for the enolization of a Ser residue where a dihydrogen phosphate ion, H_2PO_4^- , acts as a catalyst. The H_2PO_4^- ion mediates the proton transfer required for the enolization by acting simultaneously as both a general base and a general acid. Using the B3LYP density functional theory method, reaction pathways were located in the gas phase and hydration effects were evaluated by single-point calculations using the SM8 continuum model. The activation barriers calculated for the reaction pathways found were around 100 kJ mol^{-1} , which is consistent with spontaneous reactions occurring at physiological temperature. Our results are also consistent with experimental observations that Ser residue racemization occurs more readily in flexible regions in proteins.

Keywords: serine residue; racemization; nonenzymatic reaction; phosphate catalysis; dihydrogen phosphate ion; enolization; proton transfer; computational chemistry; density functional theory

1. Introduction

All common amino acids, except for glycine (Gly), have an asymmetric α -carbon atom, resulting in the occurrence of L- and D-forms. However, only L-amino acids are used in protein biosynthesis. Once biosynthesized, proteins, especially long-lived ones, can undergo various spontaneous reactions which are nonenzymatic and have relevance to aging and age-related diseases such as cataract and Alzheimer's disease [1–6]. Among such reactions, racemization (or epimerization if viewed from the entire protein molecule) of amino acid residues, by which D-amino acid residues gradually accumulate, has recently attracted increasing attention [7–11].

Aspartic acid (Asp) residues are the most racemization-prone amino acid residues. This is due to the well-known succinimide-mediated mechanism [12–15]. In this mechanism, the actual species undergoing racemization is a succinimide intermediate which is formed from an L-Asp residue by an intramolecular cyclization with the loss of a water molecule. As a result of this mechanism, Asp racemization is coupled to the isomerization to the β -form, so that L- β -Asp, D-Asp, and D- β -Asp residues can be formed from the original L-Asp residue. These unusual amino acid residues can also be formed from asparagine (Asn) residues, since a succinimide intermediate can also be formed from them with the loss of an ammonia molecule.

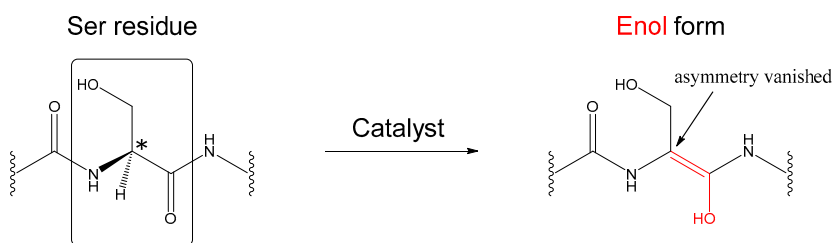
Serine (Ser) residues are the second most racemization-prone amino acid residues in an overall sense. Shapira and co-workers showed that human brain myelin basic protein (MBP), a long-lived protein, undergoes racemization at Asp and Ser residues [16,17]. High levels of racemization at Asp and

Ser residues were also found for amyloid β from Alzheimer's disease brains [17,18]. Amyloid β contains two Ser residues, Ser8 and Ser26, and both residues are probably equally racemized [19]. Kaneko and co-workers proposed possible roles of racemization of Ser26 in the pathogenesis (neurodegeneration) of Alzheimer's disease [20–24].

Age-dependent, progressive racemization of Ser residues was also found for lifelong proteins (crystallins) of normal human lenses by Hooi and Truscott [25]; by age 70, 4.5% of all Ser residues were shown to have converted to the D-form. In addition, the extent of racemization was significantly higher in cataract lenses than in age-matched normal lenses. Later, Ser59 and Ser62 residues in human α A-crystallin, the most abundant structural protein in the human lens, were demonstrated to be sites of racemization by Hooi and co-workers [26]; these two Ser residues reside in an unstructured region of the protein, and, in total, about 35% of both Ser residues were converted to the D-form in normal lenses by age 75. Once again, the extent of racemization was significantly higher in cataract lenses. Thus, racemization of Ser residues (and other spontaneous modifications) in crystallin proteins could be associated with the development of cataracts.

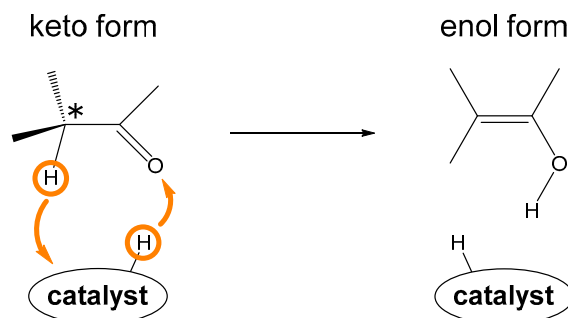
Racemization of Ser residues has also been observed for crystallin proteins from sheep, pig, and cow eye lenses, especially in structurally disordered N-terminal and C-terminal regions [27,28]. An age-dependent increase in D-Ser residues was also demonstrated for proteins in articular cartilage and tooth dentin [29,30].

Compared to Asp residue racemization, little is known about the mechanism of Ser residue racemization, although recent experimental studies using peptides suggest that a direct abstraction of the α -proton is involved in the mechanism [31,32]. A simple abstraction of the α -proton results in an enolate intermediate having a negative charge. However, at a physiological pH of 7.4, an enol species is a more likely intermediate [33–36]. The formation of the enol intermediate requires that the carbonyl oxygen of the Ser main chain be protonated (Scheme 1). Although being nonenzymatic, the enolization of a Ser residue would have to be catalyzed in order to occur at a biologically significant rate. Even two water molecules in a dimeric form may catalyze the enolization of succinimide and Ser residues [31,33–35].



Scheme 1. Enolization of the main chain of a Ser residue. The enol form, in which the asymmetry of the α -carbon has vanished, is postulated to be the intermediate of Ser residue racemization in vivo. The asterisk indicates the asymmetric α -carbon of Ser.

Recently, we have computationally shown that the racemization of the succinimide residue can be efficiently catalyzed by a dihydrogen phosphate ion, H_2PO_4^- [36]. In our proposed mechanism, this ion mediates the proton transfer required for the enolization of the $\text{H}_\alpha\text{-C}_\alpha\text{-C=O}$ moiety by acting simultaneously as both a general base and a general acid. In other words, a proton relay involving the H_2PO_4^- ion occurs, as schematically shown in Scheme 2. Our finding was consistent with the experimental observation by Tomizawa and co-workers [37] that D-Asp formation from L-Asp/L-Asn in hen egg white lysozyme was accelerated in a phosphate buffer of pH 6 (where H_2PO_4^- is the main phosphate species). The H_2PO_4^- ion also exists in a significant amount at a physiological pH of 7.4, and Ser residue racemization in vivo may also be catalyzed by this ion. Computational studies also suggest that the H_2PO_4^- ion may also have catalyzed prebiotic reactions by simultaneously acting as both a general base and a general acid [38,39]. Moreover, keto–enol tautomerism of simple aldehydes (propanal, 2-methylpropanal, and butanal) has been shown to be catalyzed by a phosphate buffer of pH 7.4 [40]. Nitro–*aci*-nitro tautomerism is also catalyzed by phosphate buffer [41].



Scheme 2. Enolization of the main chain of an amino acid residue catalyzed by a species which can act simultaneously as both a general base and a general acid (such as an H_2PO_4^- ion). The asterisk indicates the asymmetric α -carbon.

Miyamoto et al. [42] have recently reported the *in vitro* racemization of Ser residues in albumin from chicken egg white. They showed that racemization at pH 9.5 was about 4.6 times faster than at pH 7.4. This difference cannot be explained only by a specific base (OH^-) catalyzed mechanism. Since phosphate buffer was used for the experiment at pH 7.4, it is likely that a phosphate species acts as a catalyst for Ser residue racemization.

The purpose of the present study was to computationally find reasonable reaction pathways for Ser residue enolization catalyzed by an H_2PO_4^- ion. By “reasonable”, we mean that the corresponding activation barrier is around 100 kJ mol^{-1} or less, considering activation energies for typical nonenzymatic reactions of amino acid residues [12,36,43–46]. We used the model compound shown in Figure 1, where a Ser residue is capped with acetyl (Ace) and methylamino (Nme) groups on the N- and C-termini, respectively (Ace–Ser–Nme), and the B3LYP density functional theory (DFT) method. While geometry optimizations were performed in the gas phase, the effect of hydration was evaluated by single-point calculations using the SM8 (solvation model 8) continuum model [47,48], which is one of the most accurate continuum solvation models [49] and is implemented in the Spartan '14 [50] used in the present study (see Section 3 for details). We find three energetically close enolization pathways, which are consistent with *in vivo* racemization of Ser residues.

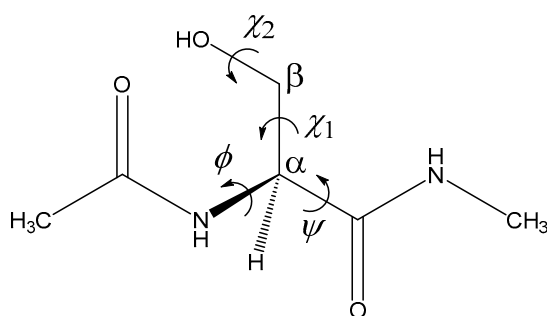


Figure 1. The model compound used in the present study (Ace–Ser–Nme, where Ace = acetyl, Ser = serine, Nme = methylamino). The φ (C–N–C $_{\alpha}$ –C) and ψ (N–C $_{\alpha}$ –C–N) dihedral angles which characterize the main-chain conformation, and the χ_1 (N–C $_{\alpha}$ –C $_{\beta}$ –O) and χ_2 (C $_{\alpha}$ –C $_{\beta}$ –O–H) dihedral angles which characterize the side-chain conformation are indicated. The Ser residue is in the L-configuration.

2. Results and Discussion

By preliminary conformational analyses for the model compound itself, we found the conformer shown in Figure 2 ($\varphi = 91^\circ$, $\psi = -124^\circ$, $\chi_1 = 80^\circ$, $\chi_2 = -63^\circ$) as one which can interact with an H_2PO_4^- ion effectively for Ser residue enolization (see Figure 1 for definition of the main-chain dihedral angles φ and ψ , and the side-chain dihedral angles χ_1 and χ_2). After the zero-point energy (ZPE), thermodynamic, and hydration Gibbs energy corrections, this conformer was the fifteenth lowest

among 23 conformers found, lying 10.0 kJ mol^{-1} above the lowest one ($\varphi = -158^\circ$, $\psi = -175^\circ$, $\chi_1 = -167^\circ$, $\chi_2 = 83^\circ$). This conformer can interact with an H_2PO_4^- ion at the three points, shown by orange circles in Figure 2, and, hence, is reactive for Ser residue enolization. It should be noted that this conformer has two intramolecular hydrogen bonds involving the Ser side chain (1.763 and 1.951 \AA) and is unique to Ser. Indeed, we did not find a corresponding stable conformation for the main chain of the analogous alanine (Ala)-containing compound (Ace-Ala-Nme); instead, a conformer with $\varphi = 73^\circ$ and $\psi = -56^\circ$ was located because of the formation of an intramolecular hydrogen bond between the oxygen of Ace and the hydrogen of Nme (1.932 \AA). It has been experimentally observed that Ser residue racemization occurs mainly in flexible regions of proteins [26–28]. Therefore, the existence of the above reactive conformer unique to Ser may be one of the reasons why Ser residues are prone to racemization. Here, it should be noted that Ser racemization reactions in lifelong proteins are very slow; their half-lives should be longer than our life spans. Therefore, these reactions need not occur in very stable Ser conformations.

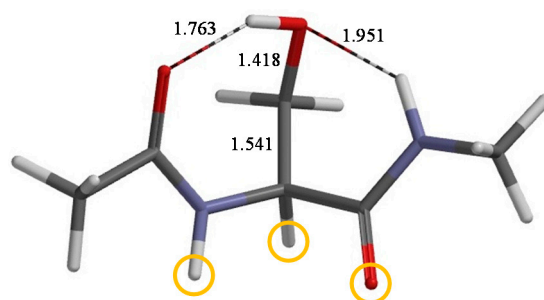


Figure 2. A conformer of the model compound shown in Figure 1 optimized by the B3LYP/6-31+G(d,p) method ($\varphi = 91^\circ$, $\psi = -124^\circ$, $\chi_1 = 80^\circ$, $\chi_2 = -63^\circ$). Selected interatomic distances are shown in \AA . This conformer can interact with an H_2PO_4^- ion at the three points indicated by orange circles and is reactive for the H_2PO_4^- -catalyzed enolization. Grey: carbon; white: hydrogen; blue: nitrogen; red: oxygen.

We identified three reaction pathways with low activation barriers, which we denote as pathway 1, pathway 2, and pathway 3. The energy profiles for these pathways are shown in Figure 3. In this figure, RC, TS, and PC stand for reactant complex, transition state, and product complex, respectively, and relative energies including the ZPE, thermodynamic, and hydration Gibbs energy corrections are shown in kJ mol^{-1} , with respect to RC1 (reactant complex of pathway 1). The optimized geometries in pathway 1, pathway 2, and pathway 3 are shown in Figures 4–6, respectively, and the dihedral angles defined in Figure 1 are reported in Table 1. Intrinsic reaction coordinate (IRC) calculations (followed by full geometry optimizations) were performed in order to confirm the connection of each transition state to the respective reactant and product complexes. The total energies, ZPEs, SM8 hydration Gibbs energies, and Cartesian coordinates of the optimized geometries are provided in Supplementary Materials.

Table 1. The main-chain dihedral angles φ and ψ , and the side-chain dihedral angles χ_1 and χ_2 (in degrees) of the optimized geometries¹.

Pathway	Geometry	φ	ψ	χ_1	χ_2
1	RC1	80	-125	79	-51
	TS1	90	-151	89	-47
	PC1	101	-157	94	-50
2	RC2	86	-126	79	-55
	TS2	98	-152	89	-52
	PC2	122	-168	94	-55
3	RC3	85	-127	79	-55
	TS3	92	-148	86	-51
	PC3	121	-167	94	-56

¹ See Figure 1 for definition of φ , ψ , χ_1 , and χ_2 .

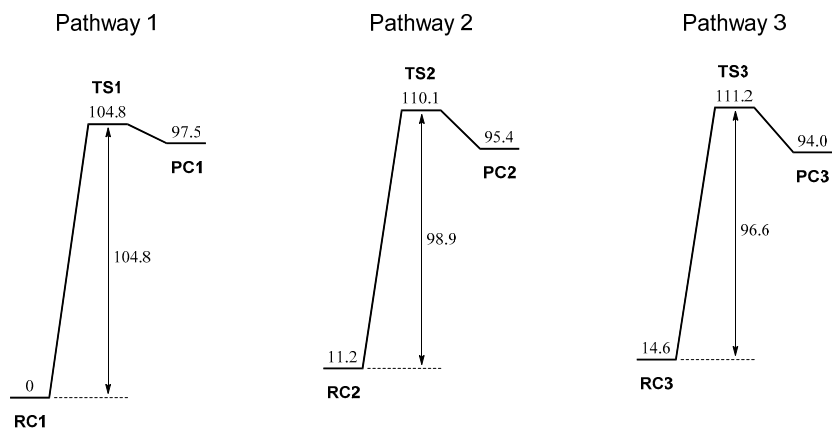


Figure 3. Energy diagrams of the three enolization pathways (pathway 1, pathway 2, and pathway 3) for the model compound. RC: reactant complex; TS: transition state; PC: product complex. The relative energies including the zero-point energy, thermodynamic, and hydration Gibbs energy corrections are shown in kJ mol^{-1} with respect to RC1 (reactant complex of pathway 1). The imaginary frequencies of TS1, TS2, and TS3 are $230i$, $151i$, and $138i \text{ cm}^{-1}$, respectively.

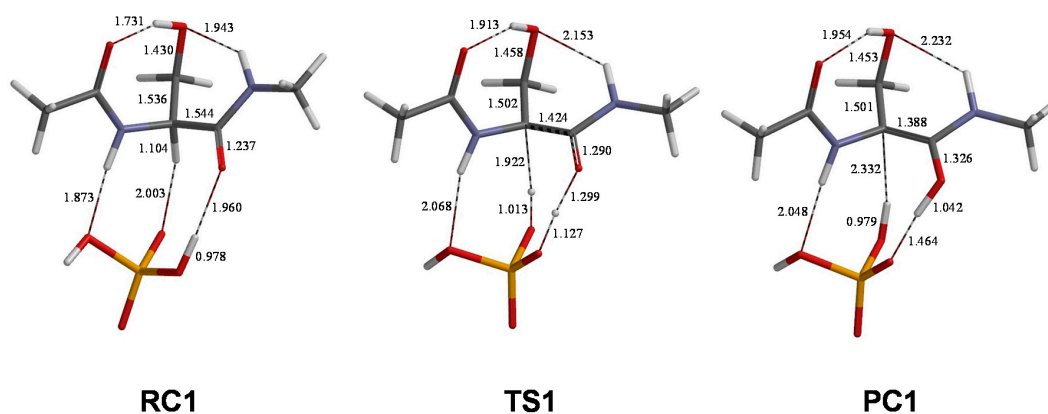


Figure 4. The geometries of RC1 (reactant complex of pathway 1), TS1 (transition state of pathway 1), and PC1 (product complex of pathway 1). Selected interatomic distances are shown in Å. Grey: carbon; white: hydrogen; blue: nitrogen; red: oxygen; orange: phosphorus.

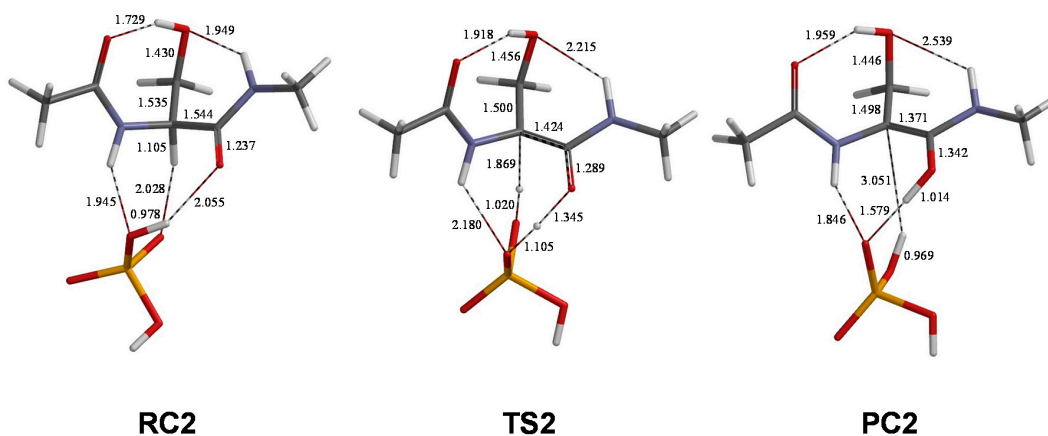


Figure 5. The geometries of RC2 (reactant complex of pathway 2), TS2 (transition state of pathway 2), and PC2 (product complex of pathway 2). Selected interatomic distances are shown in Å. Grey: carbon; white: hydrogen; blue: nitrogen; red: oxygen; orange: phosphorus.

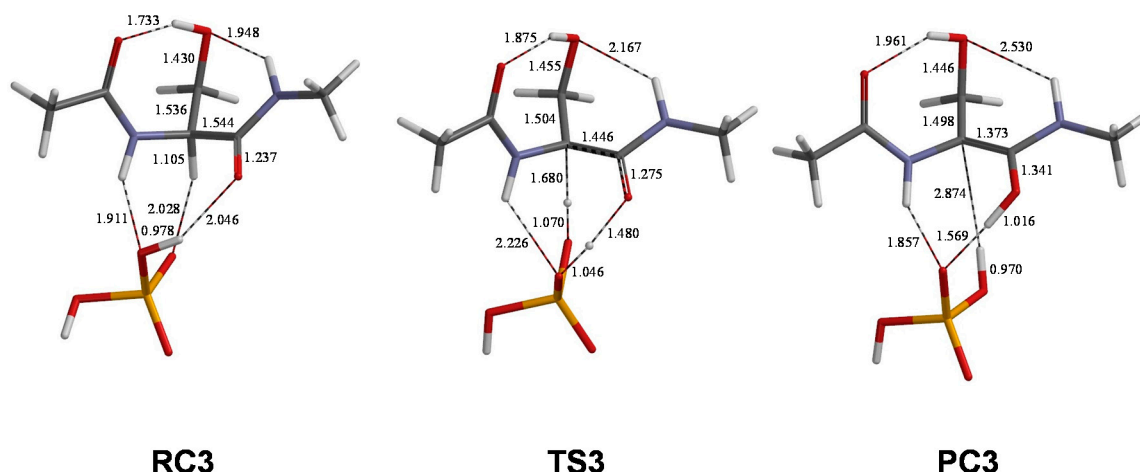


Figure 6. The geometries of RC3 (reactant complex of pathway 3), TS3 (transition state of pathway 3), and PC3 (product complex of pathway 3). Selected interatomic distances are shown in Å. Grey: carbon; white: hydrogen; blue: nitrogen; red: oxygen; orange: phosphorus.

The geometries of RC1, TS1 (transition state of pathway 1), and PC1 (product complex of pathway 1) are shown in Figure 4. In RC1, the model compound and the H_2PO_4^- ion form a complex by two hydrogen bonds and a CH–O interaction. The CH–O interaction (2.003 Å) involves the Ser $\text{C}_\alpha\text{-H}_\alpha$ bond and one of the deprotonated oxygens in H_2PO_4^- . The H_2PO_4^- ion also forms a hydrogen bond (1.960 Å) to the Ser carbonyl oxygen. The additional hydrogen bond (1.873 Å) involving the Ser NH group may also contribute to stabilizing RC1. It should be noted that the H_2PO_4^- ion in RC1 is in a pseudo- C_2 symmetry, corresponding to the global minimum geometry of an isolated H_2PO_4^- ion of C_2 symmetry [51–54].

RC1 is converted to PC1 via TS1. The corresponding activation barrier was calculated to be $104.8 \text{ kJ mol}^{-1}$ after the ZPE, thermodynamic, and hydration Gibbs energy corrections. This value is reasonable for a nonenzymatic reaction which occurs at physiological temperature. In TS1, abstraction of the Ser α -proton by the phosphate oxygen is almost completed, as may be seen from the relevant interatomic distances shown in Figure 4. On the other hand, the proton transfer from H_2PO_4^- to the carbonyl oxygen is in its early stage. Therefore, the double proton transfer mediated by the H_2PO_4^- ion is concerted but asynchronous. In TS1, the phosphate moiety has a form like an H_3PO_4 molecule. It should be noted that in TS1, the Ser $\text{C}_\alpha\text{-C}_\beta$ bond is shorter and the $\text{C}_\beta\text{-O}$ bond is longer than in RC1, indicating that the $\text{C}_\beta\text{-O}$ bond may stabilize the negative charge developing at C_α by hyperconjugation. PC1 is a complex between the enol product and an H_2PO_4^- ion formed again by a three-point interaction. In particular, the hydrogen bond between the enol hydrogen and H_2PO_4^- is very short (1.464 Å). The ψ dihedral angle changes by more than 30° by going from RC1 to PC1 (Table 1), because the C_α atom is converted to sp^2 -hybridized from sp^3 -hybridized. The relative energy of PC1 with respect to RC1 is 97.5 kJ mol^{-1} .

Figure 5 shows the geometries of RC2 (reactant complex of pathway 2), TS2 (transition state of pathway 2), and PC2 (product complex of pathway 2). In RC2, the H_2PO_4^- ion is again in a pseudo- C_2 symmetry, but the model compound interacts with the H_2PO_4^- ion in a different way from RC1 at the three points shown in Figure 2. RC2 is higher in energy than RC1 by 11.2 kJ mol^{-1} . However, the local activation barrier for pathway 2 is 98.9 kJ mol^{-1} , which is lower than for pathway 1 by 5.9 kJ mol^{-1} . Compared to TS1, the energy of TS2 is 5.3 kJ mol^{-1} higher. PC2 is only slightly more stable than PC1 by 2.1 kJ mol^{-1} . The double proton transfer mediated by the H_2PO_4^- ion is again concerted but asynchronous, as may be seen from the relevant interatomic distances shown in Figure 5. The side-chain $\text{C}_\beta\text{-O}$ bond again seems to stabilize the transition state hyperconjugatively. In pathway 2, a larger change in the main-chain conformation was observed compared to pathway 1; the φ and ψ dihedral

angles change by 36° and 42° , respectively, when going from RC2 to PC2. In PC2, the interaction between C_α and the abstracted α -proton is weak (3.051 Å).

Figure 6 shows the geometries of RC3 (reactant complex of pathway 3), TS3 (transition state of pathway 3), and PC3 (product complex of pathway 3). RC3 and RC2 can be related to each other by a proton transfer in the phosphate moiety. RC3 is higher in energy than RC2 by 3.4 kJ mol^{-1} . However, the local activation barrier of pathway 3 is 96.6 kJ mol^{-1} , which is the lowest among the three pathways. Compared to TS1 and TS2, the energy of TS3 is higher by 6.4 and 1.1 kJ mol^{-1} , respectively. PC3 is the lowest in energy among the three product complexes. In RC3, the H_2PO_4^- ion is not in a pseudo- C_2 symmetry, but in a pseudo- C_s symmetry. This is thought to be the main reason for the energy difference between RC2 and RC3 [52–54]. Interestingly, the H_2PO_4^- ion is in a pseudo- C_2 symmetry in PC3, consistent with its stability mentioned above. Since the three transition states (TS1, TS2, and TS3) have similar energies, all the three pathways may plausibly mimic the in vivo enolization of Ser residues. The changes in dihedral angles in pathway 3 are very similar to those in pathway 2. The hyperconjugation of the side-chain C_β -O bond seems to be also operative in pathway 3. Compared to TS1 and TS2, TS3 has a shorter distance of the cleaving C_α -H $_\alpha$ bond (1.680 Å) and a longer distance of the forming enol O-H bond (1.480 Å).

3. Computational Details

Figure 1 shows the model compound used in the present study (Ace-Ser-Nme), in which a Ser residue is capped with acetyl and methylamino groups on the N- and C-termini, respectively. Searches for the reaction pathways of Ser residue enolization were performed for complexes between the model compound and an H_2PO_4^- ion. All calculations were carried out by DFT with the B3LYP functional using Spartan '14 [50]. Geometry optimizations and vibrational frequency calculations were performed using the 6-31+G(d,p) basis set in the gas phase. Moreover, hydration Gibbs energies were evaluated at the gas-phase optimized geometries using the SM8 continuum model [47,48], as implemented in Spartan '14; the 6-31G(d) basis set was employed for these calculations because it gives stable atomic charges and is recommended by the developers of the model [55]. All the optimized geometries were confirmed to be an energy minimum (with no imaginary frequency) or a transition state (with a single imaginary frequency) by the vibrational frequency calculations. The relative energies reported in this paper include the ZPE and thermodynamic corrections to give the Gibbs energy at 298.15 K and 1 atm, and the SM8 hydration Gibbs energy correction. IRC calculations (followed by full geometry optimizations) were performed from all the transition states to confirm the energy minima connected by each transition state.

4. Conclusions

We have computationally found plausible reaction pathways for Ser residue enolization where an H_2PO_4^- ion acts as a catalyst. As in the previous study for the racemization of a succinimide residue [36], the H_2PO_4^- ion acts both as a general base and a general acid in a single step. More specifically, it abstracts the α -proton from the Ser residue, and donates a proton of its own to the Ser carbonyl oxygen. It seems that an H_2PO_4^- ion has an effective proton relay ability. It has recently been elucidated that the majority of Ser (and Asp) residues that are susceptible to racemization reside in flexible regions of proteins [26–28]. If a Ser residue can adopt such a conformation as shown in Figure 2 and then its α -proton and carbonyl oxygen are exposed to solvent water, it is likely to undergo enolization (and hence racemization) by the mechanism revealed in the present study. At physiological pH, there exist more HPO_4^{2-} ions than H_2PO_4^- . It would be interesting to know which ion catalyzes the enolization of Ser (and other residues) more effectively, especially in the context of aging and pathologies. In order to elucidate the relative catalytic abilities of H_2PO_4^- and HPO_4^{2-} , calculations including at least several explicit water molecules will be needed. We are now planning such calculations.

Supplementary Materials: The following are available online at www.mdpi.com/2073-4344/7/12/363/s1, Table S1: Total energies (au), zero-point energies (kJ mol⁻¹), and SM8 hydration Gibbs energies (kJ mol⁻¹) of the B3LYP/6-31+G(d,p) optimized geometries, Table S2: Cartesian coordinates (Å) of RC1, Table S3: Cartesian coordinates (Å) of TS1, Table S4: Cartesian coordinates (Å) of PC1, Table S5: Cartesian coordinates (Å) of RC2, Table S6: Cartesian coordinates (Å) of TS2, Table S7: Cartesian coordinates (Å) of PC2, Table S8: Cartesian coordinates (Å) of RC3, Table S9: Cartesian coordinates (Å) of TS3, Table S10: Cartesian coordinates (Å) of PC3.

Acknowledgments: The authors would like to acknowledge Tohoku Medical and Pharmaceutical University for financial support.

Author Contributions: O.T. conceived and designed the calculations; O.T., R.K., and N.M. performed the calculations; O.T. wrote the paper.

Conflicts of Interest: The authors declare no conflict of interest.

References

1. Cloos, P.A.C.; Christgau, S. Non-enzymatic covalent modifications of proteins: Mechanisms, physiological consequences and clinical applications. *Matrix Biol.* **2002**, *21*, 39–52. [[CrossRef](#)]
2. Hipkiss, A.R. Non-oxidative modification of DNA and proteins. In *Aging at the Molecular Level*; von Zglinicki, T., Ed.; Kluwer Academic Publishers: Dordrecht, The Netherlands, 2003; pp. 145–177. ISBN 1-4020-1738-3.
3. Hipkiss, A.R. Accumulation of altered proteins and ageing: Causes and effects. *Exp. Gerontol.* **2006**, *41*, 464–473. [[CrossRef](#)] [[PubMed](#)]
4. Truscott, R.J.W. Are ancient proteins responsible for the age-related decline in health and fitness? *Rejuvenation Res.* **2010**, *13*, 83–89. [[CrossRef](#)] [[PubMed](#)]
5. Truscott, R.J.W.; Friedrich, M.G. The etiology of human age-related cataract. Proteins don't last forever. *Biochim. Biophys. Acta* **2016**, *1860*, 192–198. [[CrossRef](#)] [[PubMed](#)]
6. Truscott, R.J.W.; Schey, K.L.; Friedrich, M.G. Old proteins in man: A field in its infancy. *Trends Biochem. Sci.* **2016**, *41*, 654–664. [[CrossRef](#)] [[PubMed](#)]
7. Ritz-Timme, S.; Collins, M.J. Racemization of aspartic acid in human proteins. *Ageing Res. Rev.* **2002**, *1*, 43–59. [[CrossRef](#)]
8. Ritz-Timme, S.; Laumeier, I.; Collins, M.J. Aspartic acid racemization: Evidence for marked longevity of elastin in human skin. *Br. J. Dermatol.* **2003**, *149*, 951–959. [[CrossRef](#)] [[PubMed](#)]
9. Fujii, N. D-Amino acid in elderly tissues. *Biol. Pharm. Bull.* **2005**, *28*, 1585–1589. [[CrossRef](#)] [[PubMed](#)]
10. Fujii, N.; Kaji, Y.; Fujii, N. D-Amino acids in aged proteins: Analysis and biological relevance. *J. Chromatogr. B* **2011**, *879*, 3141–3147. [[CrossRef](#)] [[PubMed](#)]
11. Fujii, N.; Takata, T.; Fujii, N.; Aki, K.; Sakaue, H. D-Amino acid residues in proteins related to aging and age-related diseases and a new analysis of the isomers in proteins. In *D-Amino Acids: Physiology, Metabolism, and Application*; Yoshimura, T., Nishikawa, T., Homma, H., Eds.; Springer: Tokyo, Japan, 2016; pp. 241–254. ISBN 978-4-431-56075-3.
12. Geiger, T.; Clarke, S. Deamidation, isomerization, and racemization at asparaginyl and aspartyl residues in peptides. Succinimide-linked reactions that contribute to protein degradation. *J. Biol. Chem.* **1987**, *262*, 785–794. [[PubMed](#)]
13. Stephenson, R.C.; Clarke, S. Succinimide formation from aspartyl and asparaginyl peptides as a model for the spontaneous degradation of proteins. *J. Biol. Chem.* **1989**, *264*, 6164–6170. [[PubMed](#)]
14. Radkiewicz, J.L.; Zipse, H.; Clarke, S.; Houk, K.N. Accelerated racemization of aspartic acid and asparagine residues via succinimide intermediates: An ab initio theoretical exploration of mechanism. *J. Am. Chem. Soc.* **1996**, *118*, 9148–9155. [[CrossRef](#)]
15. Aki, K.; Fujii, N.; Fujii, N. Kinetics of isomerization and inversion of aspartate 58 of α A-crystallin peptide mimics under physiological conditions. *PLoS ONE* **2013**, *8*, e58515. [[CrossRef](#)] [[PubMed](#)]
16. Shapira, R.; Chou, C.-H.J. Differential racemization of aspartate and serine in human myelin basic protein. *Biochem. Biophys. Res. Commun.* **1987**, *146*, 1342–1349. [[CrossRef](#)]
17. Shapira, R.; Austin, G.E.; Mirra, S.S. Neuritic plaque amyloid in Alzheimer's disease is highly racemized. *J. Neurochem.* **1988**, *50*, 69–74. [[CrossRef](#)] [[PubMed](#)]

18. Roher, A.E.; Lowenson, J.D.; Clarke, S.; Wolkow, C.; Wang, R.; Cotter, R.J.; Reardon, I.M.; Zürcher-Neely, H.A.; Henrikson, R.L.; Ball, M.J.; et al. Structural alterations in the peptide backbone of β -amyloid core protein may account for its deposition and stability in Alzheimer's disease. *J. Biol. Chem.* **1993**, *268*, 3072–3083. [[PubMed](#)]
19. Lowenson, J.D.; Clarke, S.; Roher, A.E. Chemical modifications of deposited amyloid- β peptides. *Methods Enzymol.* **1999**, *309*, 89–105. [[PubMed](#)]
20. Kaneko, I.; Yamada, N.; Sakuraba, Y.; Kamenosono, M.; Tutumi, S. Suppression of mitochondrial succinate dehydrogenase, a primary target of β -amyloid, and its derivative racemized at Ser residue. *J. Neurochem.* **1995**, *65*, 2585–2593. [[CrossRef](#)] [[PubMed](#)]
21. Kaneko, I.; Yamada, N.; Usui, Y.; Oda, T. Possible involvement of β -amyloids racemized at Ser residue in Alzheimer's disease. In *Alzheimer's Disease: Biology, Diagnosis and Therapeutics*; Iqbal, K., Winblad, B., Nishimura, T., Takeda, M., Wisniewski, H.M., Eds.; Wiley: Chichester, UK, 1997; pp. 519–528. ISBN 0-471-96964-8.
22. Kaneko, I.; Morimoto, K.; Kubo, T. Drastic neuronal loss *in vivo* by β -amyloid racemized at Ser²⁶ residue: Conversion of non-toxic [D-Ser²⁶] β -amyloid 1–40 to toxic and proteinase-resistant fragments. *Neuroscience* **2001**, *104*, 1003–1011. [[CrossRef](#)]
23. Kubo, T.; Nishimura, S.; Kumagai, Y.; Kaneko, I. In vivo conversion of racemized β -amyloid ([D-Ser²⁶]A β 1–40) to truncated and toxic fragments ([D-Ser²⁶]A β 25–35/40) and fragment presence in the brains of Alzheimer's patients. *J. Neurosci. Res.* **2002**, *70*, 474–483. [[CrossRef](#)] [[PubMed](#)]
24. Kubo, T.; Kumagai, Y.; Miller, C.A.; Kaneko, I. β -Amyloid racemized at the Ser²⁶ residue in the brains of patients with Alzheimer disease: Implications in the pathogenesis of Alzheimer disease. *J. Neuropathol. Exp. Neurol.* **2003**, *62*, 248–259. [[CrossRef](#)] [[PubMed](#)]
25. Hooi, M.Y.S.; Truscott, R.J.W. Racemisation and human cataract. D-Ser, D-Asp/Asn and D-Thr are higher in the lifelong proteins of cataract lenses than in age-matched normal lenses. *AGE* **2011**, *33*, 131–141. [[CrossRef](#)] [[PubMed](#)]
26. Hooi, M.Y.S.; Raftery, M.J.; Truscott, R.J.W. Age-dependent racemization of serine residues in a human chaperone protein. *Protein Sci.* **2013**, *22*, 93–100. [[CrossRef](#)] [[PubMed](#)]
27. Tao, Y.; Julian, R.R. Identification of amino acid epimerization and isomerization in crystallin proteins by tandem LC-MS. *Anal. Chem.* **2014**, *86*, 9733–9741. [[CrossRef](#)] [[PubMed](#)]
28. Lyon, Y.A.; Sabbah, G.M.; Julian, R.R. Identification of sequence similarities among isomerization hotspots in crystallin proteins. *J. Proteosome Res.* **2017**, *16*, 1797–1805. [[CrossRef](#)] [[PubMed](#)]
29. Stabler, T.V.; Byers, S.S.; Zura, R.D.; Kraus, V.B. Amino acid racemization reveals differential protein turnover in osteoarthritic articular and meniscal cartilages. *Arthritis Res. Ther.* **2009**, *11*, R34. [[CrossRef](#)] [[PubMed](#)]
30. Cloos, P.A.C.; Jensen, A.L. Age-related de-phosphorylation of proteins in dentin: A biological tool for assessment of protein age. *Biogerontology* **2000**, *1*, 341–356. [[CrossRef](#)] [[PubMed](#)]
31. Demarchi, B.; Collins, M.; Bergström, E.; Dowle, A.; Penkman, K.; Thomas-Oates, J.; Wilson, J. New experimental evidence for in-chain amino acid racemization of serine in a model peptide. *Anal. Chem.* **2013**, *85*, 5835–5842. [[CrossRef](#)] [[PubMed](#)]
32. Lyons, B.; Jamie, J.F.; Truscott, R.J.W. Separate mechanisms for age-related truncation and racemisation of peptide-bound serine. *Amino Acids* **2014**, *46*, 199–207. [[CrossRef](#)] [[PubMed](#)]
33. Takahashi, O.; Kobayashi, K.; Oda, A. Modeling the enolization of succinimide derivatives, a key step of racemization of aspartic acid residues: Importance of a two-H₂O mechanism. *Chem. Biodiv.* **2010**, *7*, 1349–1356. [[CrossRef](#)] [[PubMed](#)]
34. Takahashi, O.; Kobayashi, K.; Oda, A. Computational insight into the mechanism of serine residue racemization. *Chem. Biodiv.* **2010**, *7*, 1625–1629. [[CrossRef](#)] [[PubMed](#)]
35. Takahashi, O. Two-water-assisted racemization of the succinimide intermediate formed in proteins. A computational model study. *Health* **2013**, *5*, 2018–2021. [[CrossRef](#)]
36. Takahashi, O.; Kirikoshi, R.; Manabe, N. Racemization of the succinimide intermediate formed in proteins and peptides: A computational study of the mechanism catalyzed by dihydrogen phosphate ion. *Int. J. Mol. Sci.* **2016**, *17*, 1698. [[CrossRef](#)] [[PubMed](#)]
37. Tomizawa, H.; Yamada, H.; Wada, K.; Imoto, T. Stabilization of lysozyme against irreversible inactivation by suppression of chemical reactions. *J. Biochem.* **1995**, *117*, 635–640. [[CrossRef](#)] [[PubMed](#)]
38. Šponer, J.E.; Šponer, J.; Fuentes-Cabrera, M. Prebiotic routes to nucleosides: A quantum chemical insight into the energetics of the multistep reaction pathways. *Chem. Eur. J.* **2011**, *17*, 847–854. [[CrossRef](#)] [[PubMed](#)]

39. Szabla, R.; Šponer, J.E.; Šponer, J.; Góra, R.W. Theoretical studies of the mechanism of 2-aminooxazole formation under prebiotically plausible conditions. *Phys. Chem. Chem. Phys.* **2013**, *15*, 7812–7818. [[CrossRef](#)] [[PubMed](#)]
40. Bohne, C.; MacDonald, I.D.; Dunford, H.B. Measurement of rates and equilibria for keto–enol tautomerism of aldehydes using horseradish peroxidase compound I. *J. Am. Chem. Soc.* **1986**, *108*, 7867–7868. [[CrossRef](#)] [[PubMed](#)]
41. Bora, P.P.; Bez, G. Henry reaction in aqueous media at neutral pH. *Eur. J. Org. Chem.* **2013**, *2013*, 2922–2929. [[CrossRef](#)]
42. Miyamoto, T.; Takahashi, N.; Sekine, M.; Ogawa, T.; Hidaka, M.; Homma, H.; Masaki, H. Transition of serine residues to the D-form during the conversion of ovalbumin into heat stable S-ovalbumin. *J. Pharm. Biomed. Anal.* **2015**, *116*, 145–149. [[CrossRef](#)] [[PubMed](#)]
43. Fujii, N.; Momose, Y.; Harada, K. Kinetic study of racemization of aspartyl residues in model peptides of α A-crystallin. *Int. J. Pept. Protein Res.* **1996**, *48*, 118–122. [[CrossRef](#)] [[PubMed](#)]
44. Patel, K.; Borchardt, R.T. Chemical pathways of peptide degradation. II. Kinetics of deamidation of an asparaginyl residue in a model hexapeptide. *Pharm. Res.* **1990**, *7*, 703–711. [[CrossRef](#)] [[PubMed](#)]
45. Patel, K.; Borchardt, R.T. Chemical pathways of peptide degradation. III. Effect of primary sequence on the pathways of deamidation of asparaginyl residues in hexapeptides. *Pharm. Res.* **1990**, *7*, 787–793. [[CrossRef](#)] [[PubMed](#)]
46. Connolly, B.D.; Tran, B.; Moore, J.M.R.; Sharma, V.K.; Kosky, A. Specific catalysis of asparaginyl deamidation by carboxylic acids: Kinetic, thermodynamic, and quantitative structure–property relationship analyses. *Mol. Pharm.* **2014**, *11*, 1345–1358. [[CrossRef](#)] [[PubMed](#)]
47. Marenich, A.V.; Olson, R.M.; Kelly, C.P.; Cramer, C.J.; Truhlar, D.G. Self-consistent reaction field model for aqueous and nonaqueous solutions based on accurate polarized partial charges. *J. Chem. Theory Comput.* **2007**, *3*, 2011–2033. [[CrossRef](#)] [[PubMed](#)]
48. Cramer, C.J.; Truhlar, D.G. A universal approach to solvation modeling. *Acc. Chem. Res.* **2008**, *41*, 760–768. [[CrossRef](#)] [[PubMed](#)]
49. Klamt, A.; Mennucci, B.; Tomasi, J.; Barone, V.; Curutchet, C.; Orozco, M.; Luque, F.J. On the performance of continuum solvation methods. A comment on “universal approaches to solvation modeling”. *Acc. Chem. Res.* **2009**, *42*, 489–492. [[CrossRef](#)] [[PubMed](#)]
50. Wavefunction, Inc. *Spartan '14*; Version 1.1.4; Wavefunction, Inc.: Irvine, CA, USA, 2014.
51. Hayes, D.M.; Kollman, P.A.; Rothenberg, S. A conformational analysis of H_3PO_4 , H_2PO_4^- , HPO_4^{2-} and related model compounds. *J. Am. Chem. Soc.* **1977**, *99*, 2150–2154. [[CrossRef](#)]
52. Ma, B.; Xie, Y.; Shen, M.; Schleyer, P.V.R.; Schaefer, H.F., III. Isomerization of $\text{PO}_3^-(\text{H}_2\text{O})_n$ clusters to $\text{H}_2\text{PO}_4^-(\text{H}_2\text{O})_{n-1}$: Transition states and barrier heights. *J. Am. Chem. Soc.* **1993**, *115*, 11169–11179. [[CrossRef](#)]
53. Wang, X.-B.; Vorpapel, E.R.; Yang, X.; Wang, L.-S. Experimental and theoretical investigations of the stability, energetics, and structures of H_2PO_4^- , $\text{H}_2\text{P}_2\text{O}_7^{2-}$, and $\text{H}_3\text{P}_3\text{O}_{10}^{2-}$ in the gas phase. *J. Phys. Chem. A* **2001**, *105*, 10468–10474. [[CrossRef](#)]
54. Brandán, S.A.; Díaz, S.B.; González, J.J.L.; Disalvo, E.A.; Altabef, A.B. Experimental and theoretical study of the hydration of phosphate groups in esters of biological interest. *Spectrochim. Acta Part A* **2007**, *66*, 884–897. [[CrossRef](#)] [[PubMed](#)]
55. Chamberlin, A.C.; Cramer, C.J.; Truhlar, D.G. Performance of SM8 on a test to predict small-molecule solvation free energies. *J. Phys. Chem. B* **2008**, *112*, 8651–8655. [[CrossRef](#)] [[PubMed](#)]

